

Cu-S Coped TiO₂ NanoPhotocatalyst for the Degradation of Environmental and Industrial Pollutants

S.T. Hussain^{*1}, M. Mazhar², Asima Siddiq¹, Hina Javid² and M. Siddiq²

¹National Centre for Physics, Quaid-i-Azam University, Islamabad 43520, Pakistan

²Chemistry Dept. Quaid-i-AZam University, Islamabad 43520, Pakistan

Abstract: Sulfur doped titanium dioxide anatase nano-photocatalyst with different copper loadings (5, 10, 15, and 20 w/w %) was synthesized by hydrothermal method. The fabricated nanocatalysts were found to have high surface area, high aspect ratio, good surface morphology and high metals dispersion. The synthesized nanocatalysts were characterized by X-ray powder diffraction (XRD), Scanning electron microscopy (SEM), Diffuse reflectance spectroscopy (DRS), Fourier transform infrared spectroscopy (FTIR), Energy dispersive X-ray (EDX), Brunauer Emmett teller method (BET). The results revealed that photocatalyst possesses anatase phase having particle size in the range of 9 to 12nm. The band gap of the photocatalyst was determined using transformed diffuse reflectance spectroscopy according to the Kubelka-Munk theory, showed prominent band gap decrease with increase in the Cu loadings.

The photocatalytic activity of S-TiO₂ and copper loaded S-TiO₂ nanocatalyst were determined for degradation of phenol into hydrocarbons (methane, ethene, and propene) and photo reduction of CO₂ into ethanol. The activity results revealed that degradation of phenol and photoreduction of CO₂ increased with increasing copper loadings, due to creation of electronically modified active sites and change in the electron accepting properties of TiO₂ with Cu addition and creation of electron hole pair.

Keywords: K doped TiO₂, nano-photocatalyst, CO₂ conversion, phenol degradation, UV, sun radiation.

1. INTRODUCTION

Titanium Dioxide (TiO₂) based nonmaterials have been broadly studied as the most promising photocatalyst due to its nontoxicity, low cost, photo stability, non toxicity and high catalytic reactivity. Much attention has been paid in photocatalysis of titanium dioxide since photoinduced electrochemical decomposition of water into oxygen and hydrogen under ultraviolet light irradiation by Fujishima [1]. Nanophased TiO₂ which has a large surface area that can facilitate a fast rate of surface reactions, is a widely used wide-band-gap semiconductor which has attained considerable attention due to its distinctive applications as photocatalysts, gas sensors, solar cells and electrochemical devices [2,3]. Current research on TiO₂ is intended at understanding its strong photocatalytic activity because it has been proven to be an exceedingly efficient catalyst for energy conversion purposes and environmental remediation such as air purification, water disinfection, hazardous waste remediation [3-5].

The presence of pollutants such as CO₂, NO_x, SO_x in air, organic dyes and many other organic hydrocarbons such as phenol, formaldehyde methylene blue, reactive blue, methyl red and gasoline generated as a result of many industrial reactions have caused the severe environmental problems since couple of decades [6,7]. Titanium dioxide has sufficient band gap energies for promoting or catalyzing a

wide range of chemical reactions of environmental interest [7]. In particular it has been used to oxidize industrial pollutants and to convert them into harmless products of H₂O, alcohols and other useful hydrocarbons. Though, its practical application was limited by several factors, including the most restrictive one: it is only responsive to light radiation in the UV and near-UV range ($\lambda < 387$ nm) as it is a wide band-gap semiconductor (3.2 eV for anatase, 3.0 eV for rutile phase) [7,8]. Less than 5% of the whole radiant solar energy can be captured by pure titania [9].

There are however, a number of attempts physical and chemical processes which were devoted to design and develop a second generation of visible-light sensitive photocatalysts of titanium dioxide [10]. Until now, several strategies involving noble metal deposition, transition-metal ions doping, coupled semiconductor systems [11,12] has been reported. Recently an innovative technique involves the doping of TiO₂ with anions such as carbon, nitrogen, phosphorous, sulfur and fluorine reported as a good tool in a desired band gap narrowing and an enhancement in the photodegradation efficiency under visible light [9,11]. Doping with anions not only modifies the conductivity and optical properties but also introduce new surface states that may lie close to the conduction or valence band of TiO₂. Extending the TiO₂ spectral response and of improving its photoreactivity is doped with transition metals such as Cr, V and Fe [12,13] have also been explored recently. It was believed that transition metals could act as shallow traps in the lattice of TiO₂, which benefit to suppress the recombination of photoinduced electron-hole pairs when migrating from inside of the photocatalyst to the surface

*Address correspondence to this author at the National Centre for Physics, Quaid-i-Azam University, Islamabad 43520, Pakistan; Tel: +92-51-2077308; Fax: +92-51-2077395; E-mail: dr_tajammul@yahoo.com

[3,8]. Doping with metals and non metals were the most feasible methods for improving the photocatalytic activity of titania [9]. Khan *et al.* [14] reported that the photocatalytic degradation of toluene by using Boron and Carbon co-doped titania nanoparticles. Zhao *et al.* [15] reported that photocatalytic response of titania could be enhanced by using B–Ni co-doped photocatalyst by the modified sol–gel method. They proposed that Boron incorporated into TiO₂ extends the spectral response to the visible region while Ni doping could greatly enhance the photocatalytic activity. Balek *et al.* [16] reported N and F co-doped titania photocatalyst for acetaldehyde decomposition. They investigated the effects of N-F co-doping on photocatalytic activity in detail and elucidated the reasons for exhibiting the photocatalytic activity under visible light. Yin *et al.* [17] synthesized F and Zn co-doped TiO₂ nanopowders for improving the photocatalytic performance. Wei *et al.* [18] reported the preparation boron and cerium co-doped TiO₂ for extending spectral response to the visible light region and pointed out that the photocatalytic activity of Boron-Ce codoped titania was much higher than that of P25. These reports clearly indicated that modification of titania by co-doping proved to be an effective tool for enhancing its photocatalytic activity. The primary event taking place on the illuminated TiO₂ is the generation of electron-hole pairs in TiO₂. These photoionized electrons and holes are powerful reducing and oxidizing agents, which migrate to TiO₂ surface and ultimately become available for direct or indirect consecutive reduction and oxidation reactions [13,15,16].

In this study, we report the single step, size controlled fabrication of S doped and Cu-S co-doped TiO₂, and its application towards the carbon dioxide conversion to alcohol and degradation of organic waste like phenol under UV radiations. The effect of sulfur and particle size on the optical properties, degradation of phenol, conversion of carbon dioxide to alcohols were also studied for comparison. The variation in band gap was compared with the photocatalytic degradation and CO₂ conversion.

2. MATERIAL AND METHODS

2.1. Chemicals

Titanium tetrachloride purum (98.0%), Sodium hydroxide and Sulphuric acid (96%), Copper (II) chloride dihydrate (99%), Ammonium hydroxide (33%), of analytical grade were obtained from Fluka. Argon, hydrogen gas cylinders were used for preparation of sulfur and copper doped TiO₂ photocatalyst.

2.2. Preparation of S Doped TiO₂

TiO₂ nano particles were synthesized by precipitation method from TiCl₄. Fluka TiCl₄ (98% purity, Anala grade) was diluted up to 15% (1.33 M) in 15% H₂SO₄ in distilled water. The solution was stirred for two hours at room temperature. During the stirring 3M NaOH solution was added drop wise (the flow of NaOH solution was controlled through HPLC (High Performance Liquid Chromatography) during the reaction with continuous monitoring of pH. The drop wise addition of NaOH was continued until the pH of the resulting solution reached to 4, at this pH white precipitates were formed. The precipitates were then washed

with distilled water many times. Dried overnight at 100 °C. The TiO₂ powder thus obtained was calcined at 500 °C for 6 hours.

2.3. Preparation of Copper Doped TiO₂

Copper sulfur doped TiO₂ material was produced by reducing Cu²⁺ ions hydrothermally using CuCl₂ ·2H₂O along with NH₄OH. Suspensions of sulfur doped TiO₂ was prepared in distilled water. The copper dopant levels used in this work were 5%, 10%, 15%, and 20 % (w/w). In the suspensions of sulfur doped TiO₂, pre-determined amounts of CuCl₂·2H₂O and 200 ml of NH₄OH were transferred to an autoclave. The autoclave was flushed with argon, and then pressurized to 250 psi with hydrogen gas. The reactor solution was stirred and heated to 180°C for an hour. The pressure was increased from 250 psig to 500 psig upon heating. Finally autoclave was cooled to room temperature. The resulting grey powder was washed twice to remove ammonia solution and dried in the air at 110 °C, followed by calcination in air stream at 500°C for 6h. The experimental arrangement is presented in the Fig. (1).

2.4. Photocatalytic Reactions

Batch photoreactor of cylindrical shape with a capacity of 1000 ml as shown in Fig. (2) was used for the degradation of Phenol and conversion of Carbon dioxide reactions. 0.3 gms of TiO₂ nanoparticles were suspended in water with pure oxygen bubbling in case of degradation of phenol (the initial concentration of phenol was 0.1 M) while for CO₂ conversion 0.2 gm of catalyst were suspended into 0.2 N NaOH solution with pure CO₂ bubbling at the rate of 100 mls/min. In both systems a mercury lamp (Ultra-Violet Products Inc., USA; LF-204.LS), UVC (254 nm) was placed on the top of reactor to irradiate the reactor. The whole system was tightly sealed off during the irradiation, with continuous stirring using magnetic stirrer to prevent the sedimentation of the catalyst. The liquid sample was withdrawn after every two hours from reactor and analyzed using GC/MS after the chloroform extraction method.

3. CHARACTERIZATION

The crystallinity, structure and phase of samples were determined by XRD (Phillips PW 3040/60 X Pert Pro) powder diffractometer with Cu K α radiation of wavelength of 1.5406 Å. The XRD profiles were collected between 15° to 75° (2 θ) with a step size of 0.05° and step time of 3 s. The crystallite sizes of the samples were estimated from FWHM (full-width at half maximum) of XRD by Scherrer equation. Transmission Electron Microscope S-3500 N with Absorbed Electron Detector S-6542 (Hitachi Science System, Ltd), EDX (Inca Energy, Oxford Instruments Microanalysis, Ltd) under specific conditions of 20 keV, 25 mm working distance and magnification varying from x 300-1000 were used to examine the surface comparison of the samples. The Brunauer–Emmett–Teller (BET) specific surface area was determined by Nitrogen adsorption-desorption isotherms (Quantachrome Instrument, NOVA 1000 series). IR spectra were recorded on a Nicolet NEXUS 670 FTIR instrument to identify adsorbed species and / or adsorbed reaction intermediates and their structures on well dispersed catalysts and surfaces.

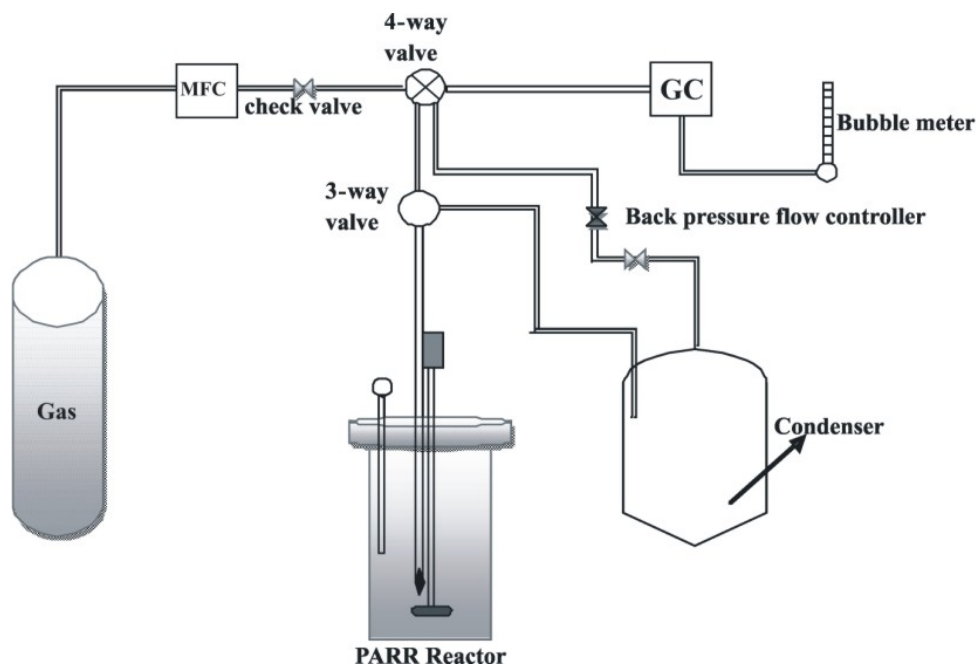


Fig. (1). Experimental arrangement of copper doped TiO₂ synthesis.

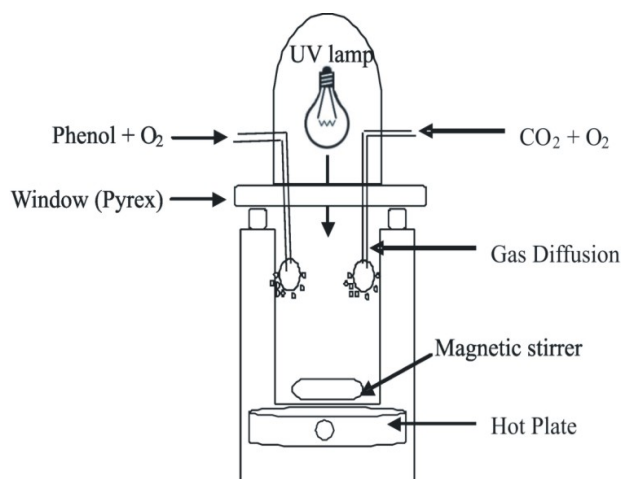


Fig. (2). Illustration of batch type reactor for Phenol and CO₂ reaction.

A (Lambda -950 Perkin-Elmer) UV-Vis spectrophotometer equipped with an integrated sphere was used to record the diffuse reflectance spectra (DRS) of the samples. The reflectance spectra of the samples were analyzed under ambient condition in the wavelength range of 200-1000 nm. The high performance liquid chromatograph pump (Shrimadau, Model LC-6A) was used for the drop wise addition of solution into the reaction mixture. The pH of reaction mixture was determined by pH meter (Inolab, Model pH 720). The chemical states and shift of the catalyst binding energies due to doping were analyzed by X-ray photoelectron spectroscopy (XPS) using a VG Microtech MT500 spectrometer, operated with a constant pass energy of 50 eV and with Mg K α radiation as the excitation source ($h\nu = 1253.6$ eV). The catalyst was pressed into a pellet, and then adhered on sample holder by carbon tape. The products of photocatalytic reactions were analyzed by using gas chromatograph (GC) (Shimadzu, Model GC-17) equipped with 30 m molecular sieve 5A plot column and a TCD detector.

4. RESULTS AND DISCUSSIONS.

4.1. XRD Studies

Fig. (3) showed the XRD patterns of prepared TiO₂ nano particles. The diffractogram of S/TiO₂ and Cu loaded S-TiO₂ showed Braggs reflection at about 25, 38, 48, 54, 63 and 75 degrees corresponding to 101, 004, 200, 211, 204, 204 tetragonal crystal planes of anatase phase of TiO₂ [19]. The presence of the anatase phase was confirmed by comparing JCPDS standard files #21-1272. Using Scherrer's formula at $\lambda = 1.5418$, $\beta = 0.774^{\circ}$, $2\theta = 24.882$, the crystallite size of all the samples were calculated and presented in Table 1. A closer look at Fig. (3) reveals that the broadening of FWHM is observed with the increase in Cu-loadings with consequent decrease in particle size and no change was observed in the crystalline form of TiO₂.

4.2. BET Measurements

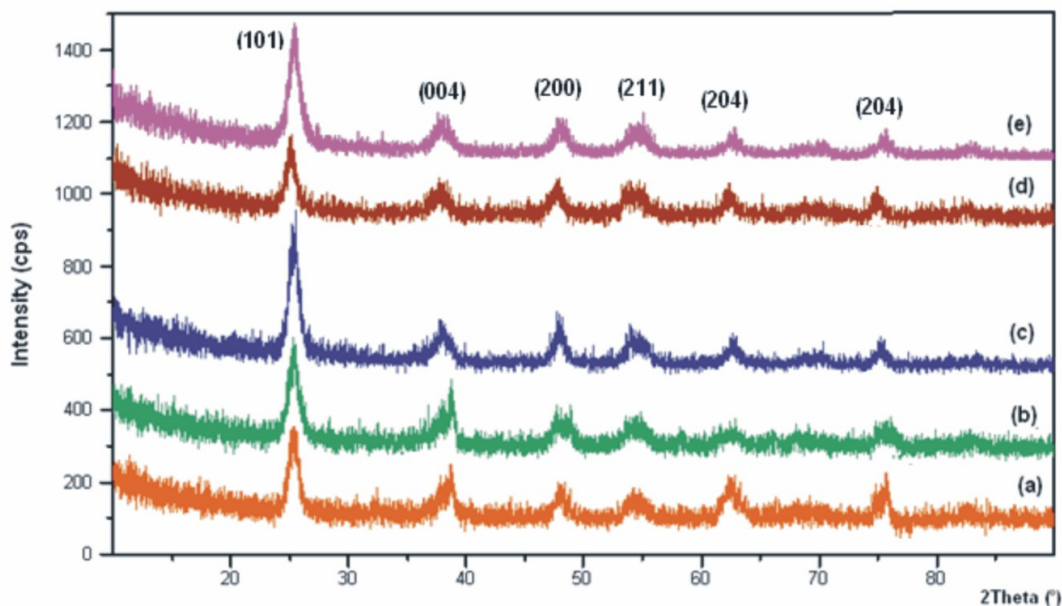
Measurements of specific surface area of all copper loaded S-TiO₂ samples are presented in Table 1, the surface area of the commercial TiO₂ is also included for comparison. It is known that BET surface area has no effect on the phase of the TiO₂ nano particles [18] but they do have an effect on the photocatalytic reaction. Larger surface area has increased adsorption/desorption capacity, consequently good photocatalytic activity [19]. As it could be seen in Table 1, copper loading significantly resulted in the increase in surface area of S/TiO₂.

4.3. SEM/EDX Studies

The surface morphology of all copper loaded S-TiO₂ samples was studied using scanning electron microscopy. Morphologies of S-doped TiO₂ and S-doped TiO₂ with various copper loadings were determined by SEM micrographs as shown in Fig. (4a-e). As seen from the SEM images, the nanoparticles are nearly round in shape and porous in nature.

Table 1. Particle Size, BET Surface Area, EDX Analysis of S-TiO₂ and S-TiO₂ Loaded with Various Copper Concentrations

Catalyst	Particle Size (nm)	BET Surface Area (m ² g ⁻¹)	EDX Analysis			
			O (%)	Ti (%)	S%	Cu%
S-TiO ₂	11.8	142	20.31	74.87	4.82	---
5% Cu loaded S-TiO ₂	11.6	178	20.28	70	4.85	4.87
10% Cu loaded S-TiO ₂	10.8	189	20.22	64.96	4.91	9.91
15% Cu loaded S-TiO ₂	10.5	215	20.27	60.09	4.86	14.78
20% Cu loaded S-TiO ₂	10	230	20.26	55.05	4.87	19.82

**Fig. (3).** XRD of (a) S-TiO₂ (b) 5% Cu loaded S-TiO₂ (c) 10% Cu loaded S-TiO₂ (d) 15% Cu loaded S-TiO₂ (e) 20% Cu loaded S-TiO₂.

EDX analysis was accomplished to assay the existence of dopant on TiO₂. Table 1 presents the EDX study of the S-doped TiO₂ and S doped TiO₂ with various copper loadings, showing the percentage of S, O, Cu and Ti confirming the formation of doped TiO₂ nano particles.

Based on the results obtained from XRD patterns, scanning electron microscopy and EDX studies, we concluded that a homogeneous surface dispersion of Cu was achieved for all doped samples.

4.4. Band Gap Measurements

UV-Vis diffuse reflectance spectroscopy was used to probe the band structure and energy levels in the crystal. The absorbance spectra of all samples were taken in the range of 200-800nm at room temperature and shown in Fig. (5). Fig. (5) represents the DRS absorbance spectra of S-TiO₂, 5% Cu loaded S-TiO₂, 10% loaded Cu loaded S-TiO₂, 15% Cu loaded S-TiO₂ and 20% Cu loaded S-TiO₂. It is evident from the above Fig. (5) that increase in the Cu loadings resulted in bathochromic shift of the absorption edge toward the visible region and decrease in the band gap of S/TiO₂ nanoparticles.

The change in the band gap with copper loadings were determined by Kubelka-Munk function $F(R)$ which is related

to the diffuse reflectance, R , of the sample and given by the following relation [19,20].

$$F(R) = (1-R)^2/2R$$

where R is the absolute value of reflectance. The energy bandgap of the samples were determined from their diffuse-reflectance spectra by plotting the square of the Kubelka-Munk function $F(R)^2$ vs Energy in electron volts. The direct energy bandgap was obtained by linear part of the curve by extrapolating to $F(R)^2 = 0$. The optical band gap energies of all samples were estimated by using the above method.

Figs. (5, 6a-c) shows the bandgap calculation of all samples determined from K-Munk function. As it is clear from Fig. (6) that energy bandgap decreases with increases Cu loadings, which are less than the S-doped sample. The band gap energies determined from the intercept of the tangents to the plots are 3.2eV for S-TiO₂, 2.9eV for 5% loaded S-TiO₂, 2.6eV 10% loaded S-TiO₂, 2.4eV for 15% loaded S-TiO₂ and 1.9eV for 20% loaded S-TiO₂. The narrowing of the band gap with increase in Cu percentage can be ascribed to Cu atom that would be incorporated into the lattice of titania, thus resulting in the change in crystalline and electronic structures [2,6,21]. In addition, this change in energy bandgap is directly reflected in the

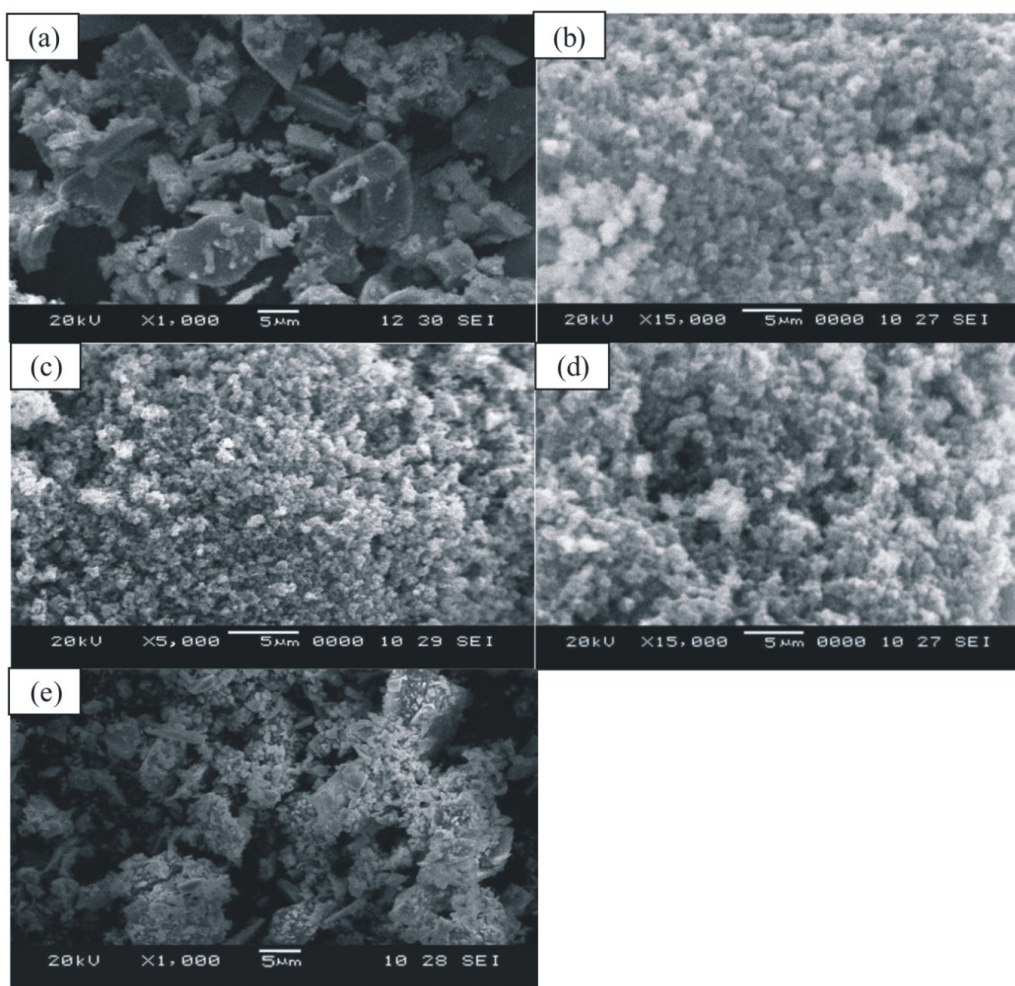


Fig. (4). (a-e): SEM micrograph of (a) S-TiO₂ (b) 5% Cu loaded S-TiO₂ (c) 10% Cu loaded S-TiO₂ (d) 15% Cu loaded S-TiO₂ (e) 20% Cu loaded S-TiO₂.

photocatalytic activity studies, where appreciable change is detected due to Cu addition.

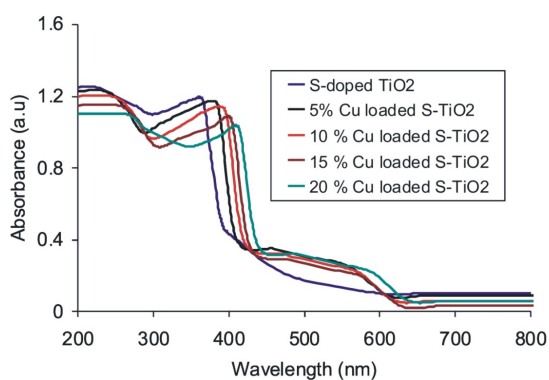


Fig. (5). Diffuse Reflectance spectra of all samples at room temperature.

4.5. FTIR Analysis

The FTIR experiments were conducted to evaluate the reaction mechanism of the catalyst and the nature of organics

present in the final products. The FTIR results of fresh and spent catalysts after phenol degradation and photo reduction of carbon dioxide are presented in Table 2. The bands appearing at 520-590 cm⁻¹ are due to stretching vibrations of M-O (Ti-O & Cu-O) and band at 1040-1060 cm⁻¹ is due to bending vibrations of Ti-S bonds in both samples [22]. The broad band peak appearing at 3200-3600 cm⁻¹ was assigned to fundamental stretching vibration of O-H hydroxyl groups (free or bonded), which are further confirmed by a weak band at about 1570-1620 cm⁻¹ which may be due to bending vibration of coordinated H₂O as well from the Ti-OH [23]. After photocatalytic activity the products were identified by growing up of absorption peaks in FTIR spectra on the surface of catalyst. The ethanol product formed after phenol degradation was identified by the appearance of vibration bands at 1340-1390 cm⁻¹, 3200-3600 cm⁻¹, 1710-1780 cm⁻¹ and 1263-1280 cm⁻¹, which are assigned to asymmetric bending vibrations of C-H and symmetric stretching vibration of O-H, C-O and C-C bonds, respectively [24], on the surface of spent catalyst. In FTIR of spent catalyst after carbon dioxide reduction absorption band in the range of 1637-1650 cm⁻¹, 1265-1280, cm⁻¹ and 1340-1390 cm⁻¹ indicates the presence of C=C, C-C and C-H group indicating the formation of some hydrocarbons intermediates

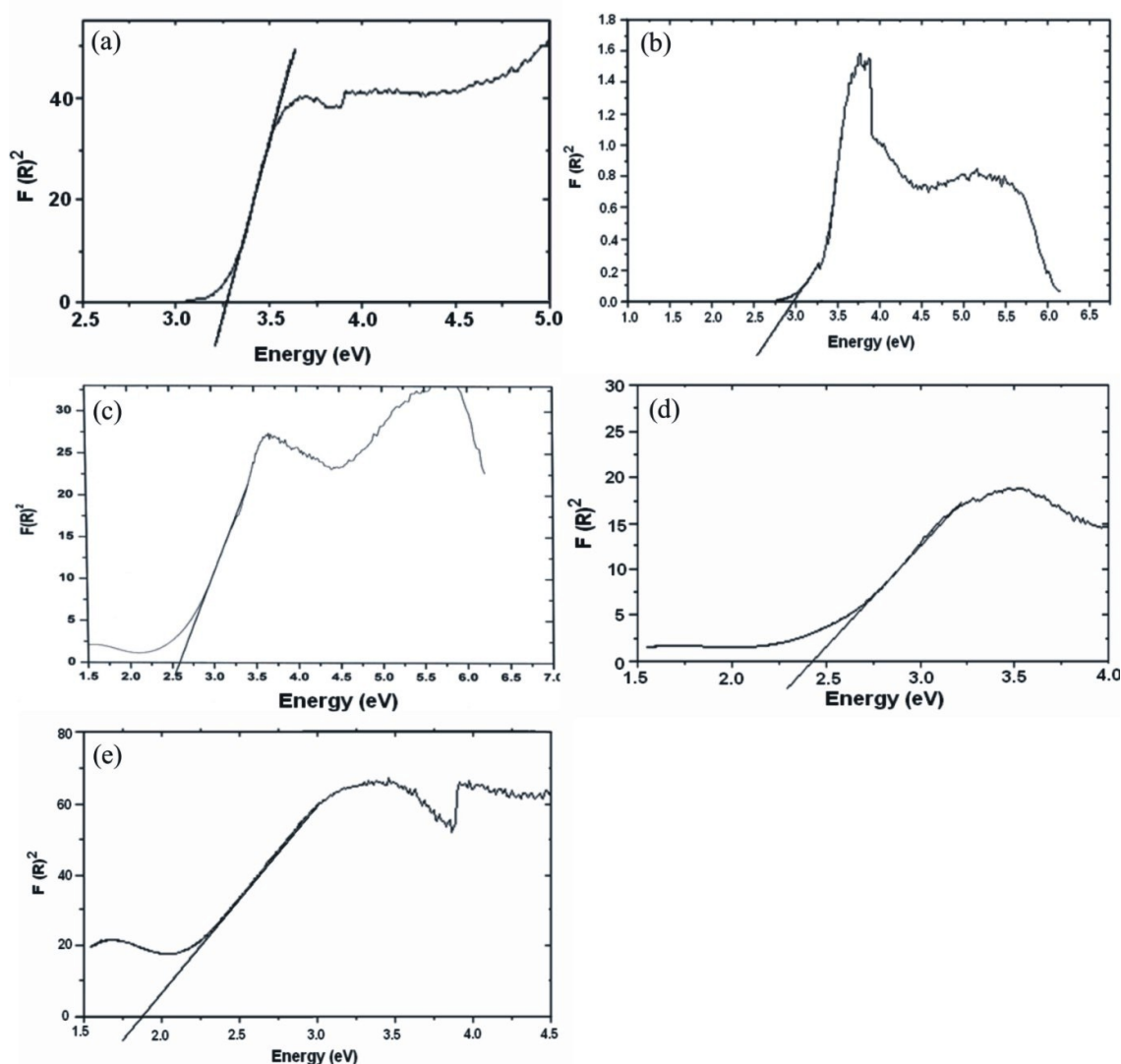


Fig. (6). Band gap measurements of (a) S-TiO₂ (b) 5% Cu loaded S-TiO₂ (c) 10% Cu loaded S-TiO₂ (d) 15% Cu loaded S-TiO₂ (e) 20% Cu loaded S-TiO₂.

on the surface of catalyst [21]. This indicates that whole catalytic process take different interaction routes on different types of active sites due to different oxidation states and phases of copper as confirmed by XPS studies. The FTIR data of fresh (F) and spent (S) catalyst before and after catalytic reaction is presented in Table 2, which supports our findings.

4.6. XPS Studies

To study the surface composition and chemical states of the synthesized catalyst, the S-TiO₂ and copper loaded S-TiO₂ were also investigated by XPS and shown in Fig. (7a, b). XPS spectra of pure TiO₂ were also studied for comparison. The individual peaks of O1s at 529.5 eV and Ti 2p at 458.2 and 463.9 eV [21,22] can be clearly seen in the high-resolution spectra (Fig. 7a, b), which mean that chemical state of the sample is Ti⁴⁺ bonded with oxygen (Ti⁴⁺-O), which has been modified after addition of S and copper. The binding energy of the Ti 2p_{3/2} and 2p_{1/2} band in case of doped Cu₂O /S-TiO₂ samples was found to be higher than that of the pure TiO₂. Increasing the copper

loadings the peaks shifted to high binding energy value as shown in Fig. (7) and Table 3. This shift towards higher side could be attributed to an atomic dispersion of copper on TiO₂ and electronically modification of TiO₂ surface geometry [20,25].

4.7. Photocatalytic Degradation of Phenol under UV Irradiations

The TiO₂ anatase is the main catalyst used in the contaminants photodegradation. However, the photocatalytic activity of TiO₂ nanoparticles have been little investigated in the literature [25,26]. In this study the photocatalytic activity of photocatalysts were evaluated in terms of degradation of phenol (1g/L) employing UV-visible spectrometry. The phenol conversion was estimated using the following formula [19,20].

$$\text{Phenol Conversion (\%)} = \frac{[\text{Phenol}]_0 - [\text{Phenol}]_t}{[\text{Phenol}]_0} \times 100 \quad (1)$$

Fig. (8) shows the degradation efficiencies of phenol versus illumination time over the different catalysts under

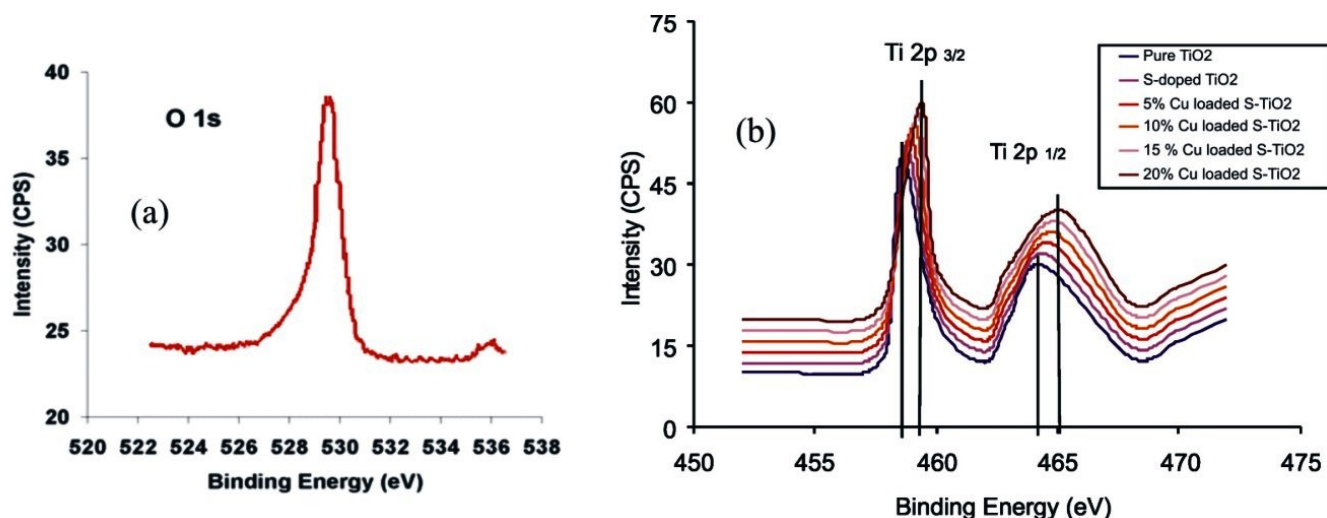
Table 2. FTIR Measurements of Fresh and Spent Catalyst

Catalyst	Functional Groups Region (cm ⁻¹)								
	Sample	M-O	O-H	Ti-S	Ti-OH	C=C	C-C	C-H	C-O
S-TiO ₂	Fresh	520	3200	1046	1620	-----	-----	-----	-----
	Spent (CO ₂ reduction)	560	3293	1040	1580	1637	1273	1345	1780
	Spent (Phenol degradation)	543	3300	1060	1600	-----	1280	1365	-----
5% Cu loaded S-TiO ₂	Fresh	537	3225	1055	1570	-----	-----	-----	-----
	Spent (CO ₂ reduction)	565	3250	1043	1575	1641	1280	1365	1755
	Spent (Phenol degradation)	550	3540	1058	1590	-----	1275	1380	-----
10% Cu loaded S-TiO ₂	Fresh	590	3410	1063	1588	-----	-----	-----	-----
	Spent (CO ₂ reduction)	529	3350	1040	1580	1640	1275	1390	1710
	Spent (Phenol degradation)	562	3595	1055	1610	-----	1263	1374	-----
15% Cu loaded S-TiO ₂	Fresh	585	3600	1043	1620	-----	-----	-----	-----
	Spent (CO ₂ reduction)	570	3320	1040	1600	1650	1265	1340	1730
	Spent (Phenol degradation)	590	3390	1045	1595	-----	1277	1350	-----
20 %Cu loaded S-TiO ₂	Fresh	525	3500	1058	1585	-----	-----	-----	-----
	Spent (CO ₂ reduction)	566	3562	1048	1605	1645	1280	1372	1780
	Spent (Phenol degradation)	541	3323	1050	1600	-----	1280	1383	-----

UV irradiations. It is clear from the Fig. (8) that the phenol degradation on the S-doped TiO₂ is less in comparison with S-doped TiO₂ photocatalyst loaded with copper, this degradation increases with increasing the copper doping. The order of photocatalytic activity was S-doped TiO₂ > 5% Cu loaded S-TiO₂ > 10 % Cu loaded S-TiO₂ > 15% Cu loaded S-TiO₂ > 20% Cu loaded S-TiO₂. About 60% phenol is degraded after 6hrs irradiation in the presence of 20% copper loaded S-TiO₂, while 5% phenol is degraded by S-TiO₂. Reaction products were analyzed after 1hr by Shimadzu (GC) gas chromatograph and shown in Fig. (9a-c). Gas samples analysis of reaction products (Fig. 9a-c) predominately showed ethane, while methane and propane were found in minor quantity. About 48.5% ethane, 18.5%

propene and 10.2% methane was obtained on 20% copper loaded sample after 6hrs while without copper S-TiO₂ showed 0.8-5% production of hydrocarbons.

We suggest that copper ions influence the photoactivity of TiO₂ by electron or hole traps, where the trap causes the formation of some active species that benefit degradation of phenol [15,16]. Cu(II) resides in the substitutional sites into the lattice of TiO₂ thus introducing a dopant energy level below the conduction band of TiO₂ and prevents the recombination of electron and hole pairs by scavenging the electron. The presence of copper dopant present at interstitial sites could create intra-band-gap states close to the valence band edges, both copper and sulfur co modification leads to a narrower band gap than S-doped TiO₂. In copper-doped

Fig. (7). XPS spectra of (a) O and (b) a S-TiO₂ with and without copper loadings.

samples, electrons are either directly trapped at Ti(IV) surface sites (form Ti^{3+}) or in deeper copper(II) sites (form Cu^{1+}). In this case, the trapped electron can be easily transferred from Cu^{1+} to a neighboring surface Ti^{4+} because of the proximity of the energy levels [10,23,25]. It could be suggested here that the S species could trap the part of photogenerated holes, thus suppressing the recombination of photogenerated electrons and holes. Moreover, Cu loaded S-TiO₂ has abundant amount of OH- group than S-TiO₂ sample, which would be beneficial for the absorption of organic compounds, capturing the photogenerated holes and formation of OH radicals (shown in Fig. 10) [26]. Furthermore the most important reason is that synergistic effects of copper and sulfur on titania may improve the separation efficiency of photogenerated electrons and holes and largely modified the photocatalytic activity under visible light irradiations. The increase in efficiencies in degradation of phenol may be attributed to the increase in copper concentration, which resulted in the increase of e-trapping by Cu^{2+} ions on Ti surface sites [27]. In the absence of Cu, the S-TiO₂ provides “weak active species” that are not effective to oxidize the organic species into products under UV irradiation [20,26]. The proposed possible mechanism for synergistic effects of copper and sulfur is presented in Fig. (10).

Table 3. Binding Energy Values of S-TiO₂ with and without Copper Loadings

Catalyst	Binding Energy Values (eV)	
	Ti 2p3/2	Ti 2p1/2
Pure TiO ₂	458.60	464.40
S-doped TiO ₂	458.75	464.55
5% Cu loaded S-TiO ₂	458.92	464.72
10% Cu loaded S-TiO ₂	459.09	464.89
15% Cu loaded S-TiO ₂	459.24	465.04
20% Cu loaded S-TiO ₂	459.39	465.19

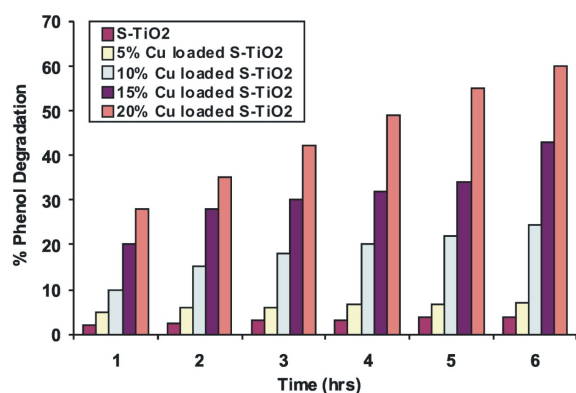


Fig. (8) Photocatalytic degradation of Phenol determined by S-TiO₂ and S-TiO₂ with various copper additions at different time rates.

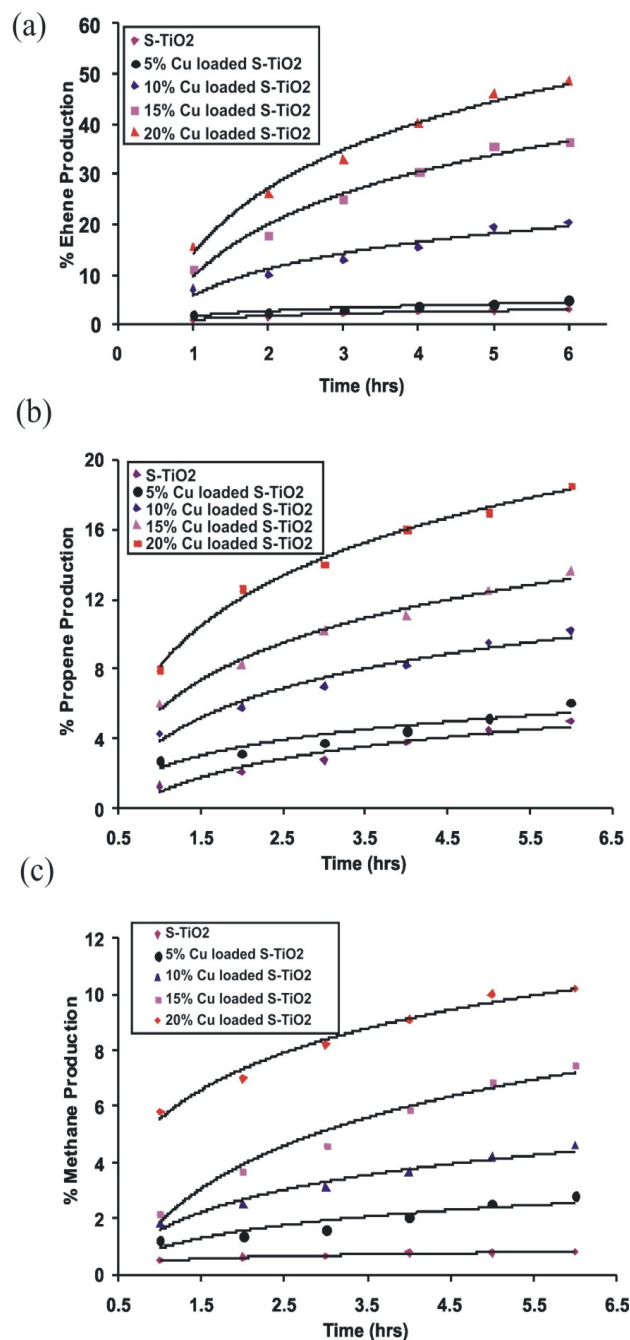


Fig. (9). Percent production (a) ethene (b) propene (c) methane by S-TiO₂ and S-TiO₂ with various copper loadings under UV and IR irradiation at room temperature at different time rates.

4.8 . Conversion of CO₂ + H₂O by Solar Energy

The photochemical conversion of CO₂ + H₂O into alcohols (ethanol) was computed after 1hr using UV radiation by S-TiO₂ and copper loaded S-TiO₂ is shown in Fig. (11). CO₂ conversion was calculated using the following formula (equation 2) [19,20].

$$CO_2 \text{ conversion (\%)} = \frac{[CO_2]_{in}}{[products]_{out}} \times 100 \quad (2)$$

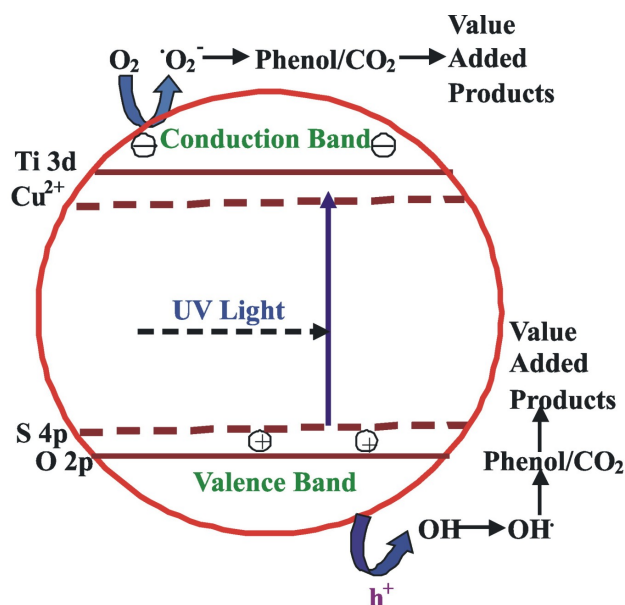


Fig. (10). The proposed photocatalytic activity mechanism.

The study of Fig. (11) clearly indicates that the conversion of CO₂ + H₂O into ethanol increases with increasing Cu loadings on S-TiO₂ nano particles and best conversion (85%) was achieved with 20% copper loaded S-TiO₂ after illumination of UV irradiations for 6hrs. Photochemical conversion of CO₂ + H₂O into ethanol follows the similar mechanism as discussed previously in section 5, Fig. (10). The electrons trapped by Cu transferred smoothly to surface where they reduce appropriate electron acceptor molecules i.e., react with oxygen molecules to form super oxide anions making the reaction exothermic while the positive holes can oxidize donor molecules i.e., break apart water molecules to form hydrogen gas and hydroxyl radicals which combines with carbon to form ethanol [25-27]. The effect of copper loadings on the ethanol selectivity is depicted in Fig. (12). The ethanol production increases with increasing copper percentage, reaching a maximum of 52% on 20% copper concentration.

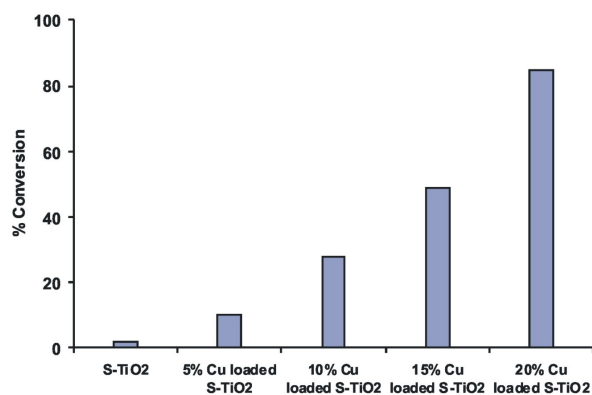


Fig. (11). Photocatalytic conversion of CO₂ + H₂O by S-TiO₂ and S-TiO₂ loaded with various copper loadings.

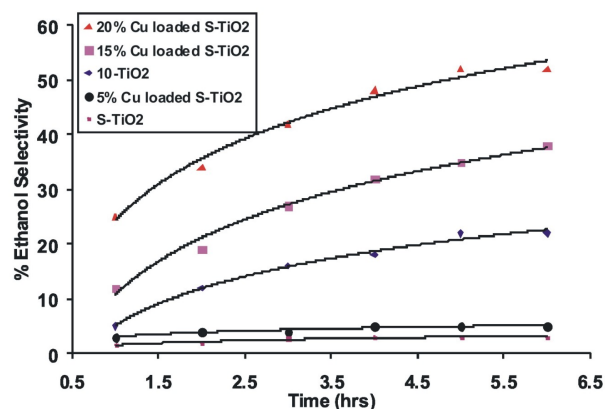


Fig. (12). % ethanol production by S-TiO₂ and S-TiO₂ loaded with various copper loadings under UV irradiations at room temperature with different time rates.

5. CONCLUSIONS

- S-doped titanium dioxide nanoparticles with various copper loadings are synthesized in a single step using hydrothermal method.
- Copper loaded S-TiO₂ photocatalyst showed high specific area, small crystallite size, narrow band gap which contribute to their high photocatalytic activity.
- The photocatalytic activity suggests that increasing copper-addition on TiO₂ resulted in increase the photocatalytic degradation of phenol and conversion of CO₂ + H₂O to alcohol.
- The copper loaded S-TiO₂ was found to be feasible and attractive to be used for further investigation of industrial and environment management studies.

ACKNOWLEDGEMENT

Declared none.

CONFLICT OF INTEREST

Declared none.

REFERENCES

- [1] Fujishima, A.; Zhang, X.; Chimie, C.R. Titanium dioxide photocatalysis: present situation and future approaches. *C. R. Chim.*, **2006**, *9*, 750-760.
- [2] Khan, M.A.; Jung, H.T.; Yang, O.B. Synthesis and characterization of ultrahigh crystalline TiO₂ nanotubes. *J. Phys. Chem. B.*, **2006**, *110*, 6626-6630.
- [3] Samarghandi, M.R.; Nouri, J.; Mesdaghinia, A.R.; Mahvi, A.H.; Nasser, S.; Vaezi, F. Efficiency removal of phenol, lead and cadmium by means of UV/ TiO₂/ H₂O₂ processes. *Int. J. Environ. Sci. Technol.*, **2007**, *4*, 19-26.
- [4] Yu, J.C.; Zhang, L.; Zheng, Z.; Zhao, J. Synthesis and characterization of phosphated titanium dioxide with high photocatalytic activity. *J. Chem. Mater.*, **2003**, *15*, 2280-2286.
- [5] Chatterjee, D.; Mahata, A. Demineralization of organic pollutants on the dye modified TiO₂ semiconductor particulate system using visible light. *J. Appl. Catal. B.*, **2001**, *33*, 119-125.
- [6] Yu, J.; Zhou, M.; Cheng, B.; Zhao, X. Preparation, characterization and photocatalytic activity of in situ N, S-codoped TiO₂ powders. *J. Mol. Catal. A. Chem.*, **2006**, *246*, 176-184.

- [7] Yu, J.C.; Yu, J.; Ho, W.; Jiang, Z.; Zhang, L. Effects of F-doping on the photocatalytic activity and microstructures of nanocrystalline TiO₂ powders. *J. Chem. Mater.*, **2002**, *14*, 3808-3816.
- [8] Anpo, M.; Takeuchi, M. The design and development of highly reactive titanium oxide photocatalysts operating under visible light irradiation. *J. Catal.*, **2003**, *216*, 505-516.
- [9] Masakazu, A. Second-generation titanium dioxide photocatalysts prepared by the application of an advanced metal ion-implantation method. *Pure. Appl. Chem.*, **2000**, *72*, 1787-1792.
- [10] Yamashita, H.; Harada, M.; Misaka, J. Application of ion beam techniques for preparation of metal ion-implanted TiO₂ thin film photocatalyst available under visible light irradiation: Metal ion implantation and ionized cluster beam method. *J. Synchrotron. Radiat.*, **2001**, *8*, 569-571.
- [11] Zhu, H.; Tao, J.; Xiang, D. Preparation and photoelectrochemical activity of Cr-doped TiO₂ nanorods with nanocavities. *J. Phys. Chem. C Nanomater. Interface*, **2010**, *114*, 2873-2879.
- [12] Wenfang, Z.; Qingju, L.; Zhongqi, Z.; Ji, Z. Preparation and properties of vanadium-doped TiO₂ photocatalysts. *J. Phys. D. Appl. Phys.*, **2010**, *43*, 035301-035305.
- [13] Cam, L.; Luu1, Q.; Tuan, N.; Si, T. Synthesis and characterization of Fe-doped TiO₂ photocatalyst by the sol-gel method. *J. Adv. Nat. Sci. Nanosci. Nanotechnol.*, **2010**, *1*, 015008-015010.
- [14] Khan, R.; Sun, W.K.; Tae-Jeong, K.; Chang, N. Comparative study of the photocatalytic performance of boron-iron Co-doped and boron-doped TiO₂ nanoparticles. *Mater. Chem. Phys.* **2008**, *112*, 167-172.
- [15] Zhao, W.; Wanhong, M.; Chuncheng, C.; Jincai, Z.; Zhigang, S. Efficient degradation of toxic organic pollutants with Ni₂O₃/TiO_{2-x}B_x under visible irradiation. *J. Am. Chem. Soc.*, **2004**, *126*, 4782-4783.
- [16] Balek, V.; Li, D.; Subrt, J.; Veernikova, E.; Hishita, S.; Mitsuhashi, T.; Haneda, H. Characterization of nitrogen and fluorine co-doped titania photocatalyst: Effect of temperature on microstructure and surface activity properties. *J. Phys. Chem. Solids*, **2007**, *68*, 770-774.
- [17] Yin, Y.; Xin, W. Preparation of F-Zn-codoped TiO₂ nanoparticles and its applications in photodegradation of methylene blue. *J. Adv. Mater. Res.*, **2009**, *79*, 329-332.
- [18] Wei, C.H.; Tang, X.H.; Liang, J.R.; Tan, S.Y. Preparation, characterization and photocatalytic activities of boron- and cerium-codoped TiO₂. *J. Environ. Sci.*, **2007**, *19*, 90-96.
- [19] Hussain, S.T.; Siddiqua, A. Iron and chromium doped titanium dioxide nanotubes for the degradation of environmental and industrial pollutants. *Int. J. Environ. Sci. Technol.*, **2011**, *8*, 351-362.
- [20] Hussain, S.T.; Khan, K.; Hussain, R. Size control synthesis of sulfur doped titanium dioxide (anatase) nanoparticles, its optical property and its photo catalytic reactivity for CO₂ + H₂O conversion and phenol degradation. *J. Nat. Gas Chem.*, **2009**, *18*, 383-391.
- [21] Lopez, T.; Moreno, J.A.; Gomez, R.; Bokhimi, X.; Wang, J.A.; Yee-Madeira, H.; Pecchi, G.; Reyes, P. Characterization of iron-doped titania sol-gel materials. *J. Mater. Chem.*, **2002**, *12*, 714-718.
- [22] Colon, G.; Maicu, M.; Hidalgo, M.C.; Navío, J.A. Cu-doped TiO₂ systems with improved photocatalytic activity. *J. Appl. Catal. B.*, **2006**, *67*, 41-45.
- [23] Ohno, T.; Akiyoshi, M.; Umebayashi, T.; Asai, K. MitSui, T.; Matsumura, M. Preparation of S-doped TiO₂ photocatalysts and their photocatalytic activities under visible light. *J. Appl. Catal. A. Gen.*, **2004**, *265*, 115-121.
- [24] Ha, S.P.; Dong, H.K.; Sun, J.K.; Kyung, S.L. The photocatalytic activity of 2.5 wt% Cu-doped TiO₂ nano powders synthesized by mechanical alloying. *J. Alloys Compd.*, **2006**, *415*, 51-55.
- [25] Bai, X.R. Preparation and photocatalytic activity of Fe-doped TiO₂ nanopowders. *J. Mater. Sci. Forum*, **2009**, *248*, 610-613.
- [26] Rungnapa, T.; Kongthip, S. Sulfur doping and its effect on TiO₂ photoactivity. *J. Sci. Technol.*, **2008**, *30*, 201-206.
- [27] Hamal, D.B.; Klabunde, K.J. Synthesis, characterization, and visible light activity of new nanoparticle photocatalysts based on silver, carbon, and sulfur doped TiO₂. *J. Colloid Interface Sci.*, **2007**, *311*, 514-522.

Received: July 6, 2011

Revised: September 20, 2011

Accepted: April 11, 2012

© Hussain et al.; Licensee Bentham Open.

This is an open access article licensed under the terms of the Creative Commons Attribution Non-Commercial License (<http://creativecommons.org/licenses/by-nc/3.0/>) which permits unrestricted, non-commercial use, distribution and reproduction in any medium, provided the work is properly cited.